

Prediction of K_m of 1,1-dichloromethane (DCM) and 1,1-dibromomethane (DBM) for DhIA mutant L263W by using COMBINE model

Motivation:

The objective of this project is to design mutant haloalkane dehalogenase with improved activity towards priority pollutant 1,1-dichloromethane for immobilization to biosensors. L263W substitution was designed by computer modelling. Here, the effect of mutation on K_m of DCM and DBM is predicted using COMBINE model.

Methods:

Preparation of DhIA L263W (DhIA01) mutants. X-ray structure of DhIA-wt (PDB accession code 2DHC) was used as a template. Seven possible rotamers of L263W (*a-g*) substitution were introduced into the wild type DhIA by PYMOL (1).

Preparation of DhIA01-DXM complexes. Orientation of DCM and DBM were taken from molecular docking to DhIA-wt (2) and inserted into DhIA01*a-g*. Geometry of the prepared complexes were energy optimised using module SANDER of the molecular mechanics programme AMBER 6.0 and the Cornell *et al.* force field. Parameters for energy minimisations were the same as used in (2).

*Prediction of K_m of DCM and DBM for DhIA01*a-g*.* Van der Waals (*vdw*) and electrostatic (*ele*) interaction energies between substrate and each amino acid were calculated using ANAL module of AMBER 6.0. The values of the *vdw* and *ele* interactions were used for prediction of K_m using COMBINE model built for DhIA-wt (2). The prediction was made in the programme SIMCA 10.

Results:

L263W rotamers. PYMOL found 14 orientations of L263W side chain. Seven of the orientations were reasonable (*a-g*) but only two of them (*c* and *g*) did not form steric clashes with neighbouring residues (Figure 1). Energy minimisation of the complexes necessarily resulted in significant (?) changes in orientation of some vicinal residues (in all cases but *c* and *g*; Table 1) and, more importantly (?) energy minimisation led to re-orientation of DCM and DBM in the active site (*c*, *e* and *g*; Table 1 and Figure 2). Orientation of L263W side chain in complexes with the rotamer *c*, *e* and *g* of the L263W does not seem to changed significantly. Rotamer *a* resembles *d* and *f*, and remotely *e*; rotamer *b* resembles *g*, and remotely *c*. Results of energy minimisations of the complexes with DCM and DBM are comparable. All rotamers of L263W decreased size of the active site cavity (ASC) compared to DhIA-wt in the following order (from the largest to the smallest ASC): $d > a > b > f > e, g > c$.

*Predicted K_m of DCM and DBM for DhIA01*a-g*.* Experimentally measured K_m constants of DCM and DBM for DhIA-wt are $\gg 100$ mM and 2,4 mM, respectively. Predicted K_m constants from COMBINE model built on DhIA-wt are 113 mM for DCM and 1,2 mM for DBM. Predicted K_m constants of DCM and DBM using interaction energies calculated for DhIA01 varies from 82 mM (DhIA01*f*) to 730 mM for DCM (DhIA01*e*) and from 1,5 mM (DhIA01*f*) to 9807 (!) mM (DhIA01*c*) for DBM (Table 2).

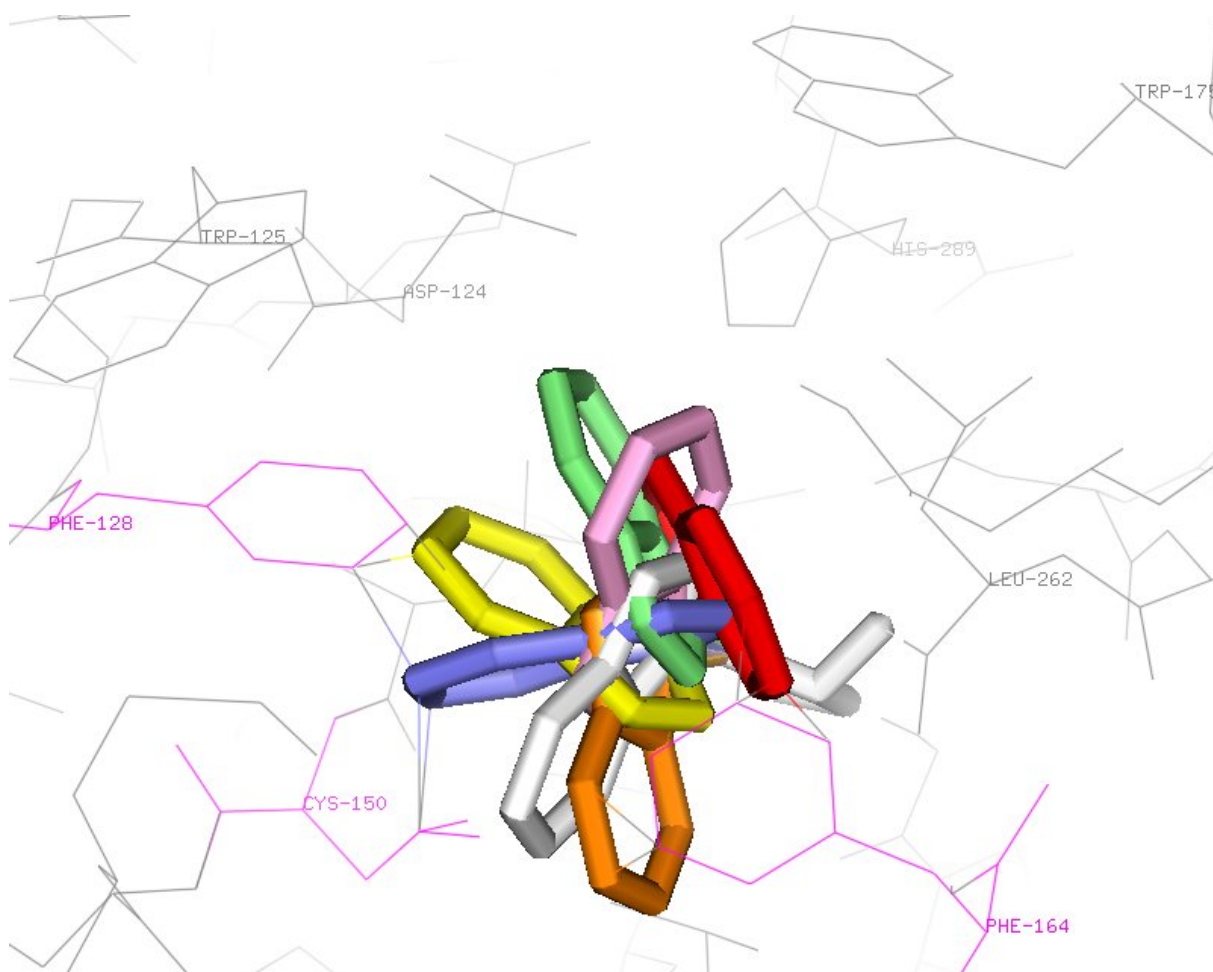


FIGURE 1 ▪ Possible rotamers (*a-g*) of L263W as reported by PYMOL. Colouring scheme is as follows: *a* (white), *b* (yellow), *c* (pink), *d* (orange), *e* (red), *f* (slate) and *g* (lime). Clashing residues are coloured and labeled in magenta. D124 (nucleophile), H289 (catalytic base), W125 (halide-stabilising residue), W175 (halide-stabilising residue) and L262 are labeled.

TABLE 1 ▪ L263W rotamers.

Rotamer	Steric clashes	Substrate	Changes caused by energy minimisation
L263Wa	C150	DCM	F164, W263
		DBM	F164, W263
L263Wb	F128	DCM	F128, W263
		DBM	F128, W263
L263Wc	-	DCM	DCM
		DBM	DBM
L263Wd	F164	DCM	F164, W263
		DBM	F164, W263
L263We	F164	DCM	DCM, F164
		DBM	DBM, F164
L263Wf	F128, C150	DCM	F128, W263
		DBM	F128, W263
L263Wg	-	DCM	DCM
		DBM	DBM

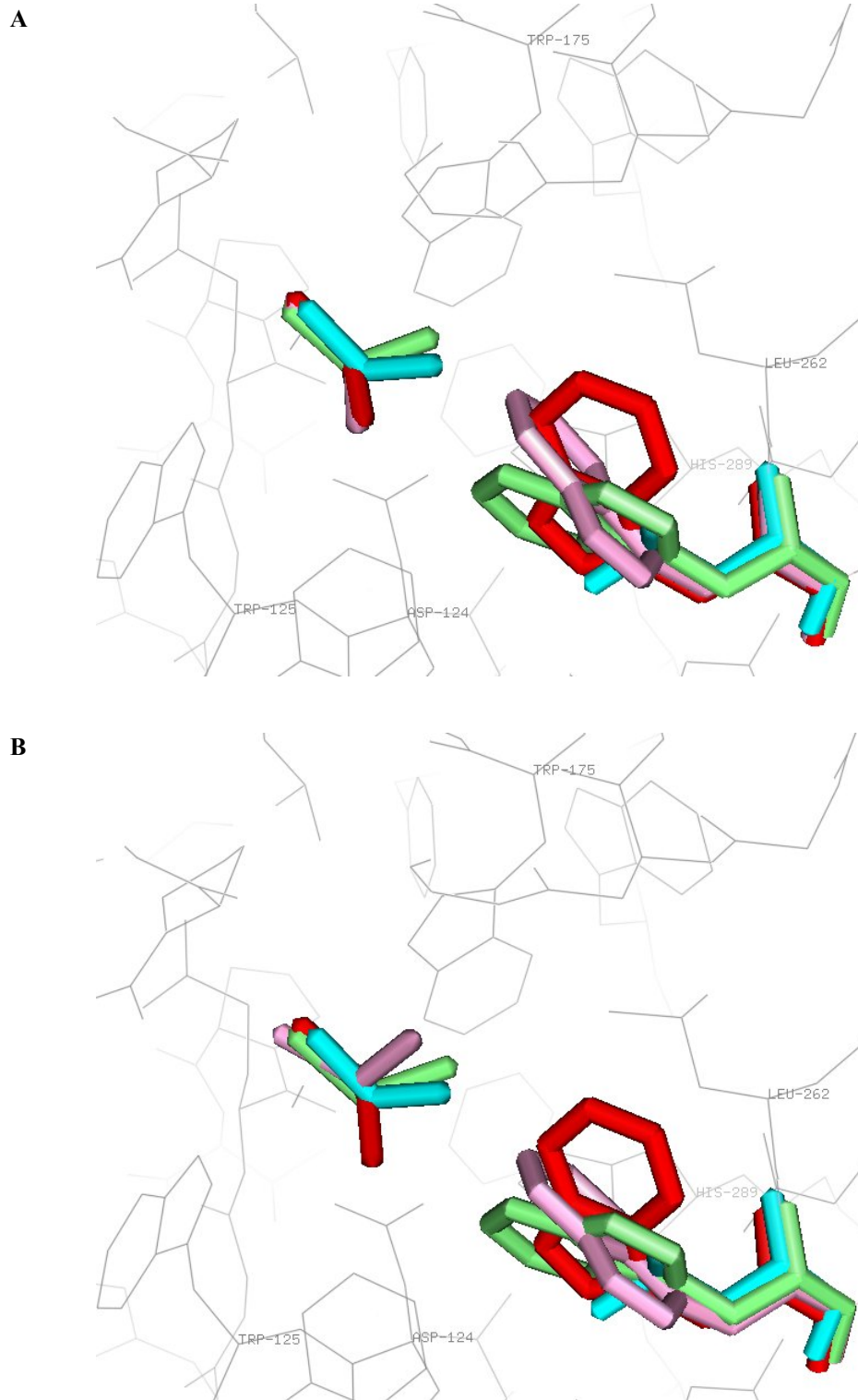


FIGURE 2 ▪ Re-orientation of DCM and DBM. A, DhIA01*c,e,g*.DCM. B, DhIA01*c,e,g*.DBM complexes. Colouring scheme is as follows: *c* (pink), *e* (red), *g* (lime). DhIA-wt residue L263, and DCM and DBM orientations are in cyan. Whole structures (grey lines) are shown only for *c* for clarity. D124 (nucleophile), H289 (catalytic base), W125 (halide-stabilising residue), W175 (halide-stabilising residue) and L262 are labeled.

TABLE 2 ■ Experimental^a and predicted^b K_m constants.

K_m	Variant	ASC size ranking ^c	DCM		DBM	
			K_m (mM)	$\log K_m$	K_m (mM)	$\log K_m$
Experiment	wt	-	100	2	2.4	0.38
	wt	8	113	2.053	1.2	0.091
Prediction	L263Wa	6	100	1.999	1.7	0.235
	L263Wb	5	219	2.341	4.4	0.642
	L263Wc	1	307	2.487	9807	3.992
	L263Wd	7	184	2.265	2.3	0.365
	L263We	2-3	730	2.864	33.5	1.525
	L263Wf	4	82	1.916	1.5	0.166
	L263Wg	2-3	165	2.217	3.0	0.477

^a(3). ^bdocking-based COMBINE model: five components; $R^2 = 0.946$; $Q^2 = 0.747$ (2).

^c1 – the smallest ASC, 8 – the largest ASC. Assigned visually.

Conclusions:

- Predicted K_m for Dh1A01 from COMBINE model built for Dh1A-wt have the same order of magnitude as the predicted K_m for DCM and DBM from Dh1A-wt regardless of substrate (DCM or DBM) and rotamer type except *c* for DBM.
- W263 might be too large residue in the case of DBM assuming possibility that W263 adopts orientation of rotamer *c*. On the other hand, further mutation may be needed to reduce the size of the active site for effective binding of DCM.
- Experimental mutagenesis (L263W) and kinetic characterisation (determination of K_m for DCM and DBM) is needed to validate predictions from the COMBINE model.

References:

1. DeLano, W.L. *The PyMol Molecular Graphics System*, DeLano Scientific LLC, San Carlos, CA, USA.
2. Kmuníček, J., Boháč, M., Luengo, S., Gago, F., Wade, R.C., and Damborský, J. (2003) *Journal of Computer-Aided Molecular Design* 17, 299-311.
3. Schanstra, J.P., Kingma, J., and Janssen, D.B. (1996) *Journal of Biological Chemistry* 271, 17474.

Construction, expression and biochemical characterization of L263W mutant of DhIA

Motivation:

Objective of this project is experimental evaluation of the effect of L263W substitution in DhIA (DhIA01) on activity towards 1,2-dichloromethane (DCM) and 1,2-dibromomethane (DBM). This mutation was designed by molecular modelling and the effect of substitution was estimated by COMBINE model (1). The results of COMBINE analysis concluded that: (i) predicted K_m for DhIA01 from COMBINE model built for DhIA-wt have the same order of magnitude as the predicted K_m for DCM and DBM from DhIA-wt regardless of substrate (DCM or DBM) and rotamer type except the rotamer *c* for DBM and (ii) W263 might be too large residue in the case of DBM assuming possibility that W263 adopts orientation of rotamer *c*. It was proposed that experimental mutagenesis and kinetic characterization is needed to validate computational design and predictions from the COMBINE analysis (1).

Methods:

Mutagenesis

Mutant recombinant gene was obtained using QuikChange™ Site-Directed Mutagenesis Kit (Stratagene, La Jolla, USA) according to manufacturer's instructions. Specific complementary primers (5'-GAAAGACAAATTGTGGGGACCGGACGTC-3') carrying substitution (in bold) were designed for mutagenesis. Plasmid pUC18 with recombinant gene *dhIA* was used as the template. Mutant recombinant gene *dhIA01* was recloned into pAQN vector (2) using *EcoRI* and *HindIII* restriction endonucleases and T4 DNA ligase (New England BioLabs, Ipswich, USA).

Expression of protein DhIA in *E. coli*

Recombinant plasmids were transformed to *E. coli* BL21 (DE3). For overexpression, cells were grown at 37 °C to an optical density about 0.6 ($\lambda = 600$ nm) in Luria-Bertani (LB) medium (Sigma-Aldrich, St. Louis, USA) with ampicillin (100 µg/ml). Cultures were incubated for approximately 3 hours at rate of 150 rpm. Protein expression was induced by adding IPTG to a final concentration 1 mM in LB medium. The temperature was decreased to 30 °C. Cells were harvested by 12 minutes centrifugation at 3700 g after 4 hours of cultivation.

Purification of protein DhIA

Cells were harvested, washed once with glycine buffer (0.1 M, pH 8.5) and then resuspended in 30 ml of glycine buffer. Harvested cells were kept at -66 °C overnight. Defrosted culture was disrupted by sonication with Soniprep 150 (Sanyo Gallenkamp, Loughborough, UK) and the lysate was centrifuged at 21000 g for one hour. The crude extract was applied to Ni-NTA Superflow column (QIAGEN, Hilden, Germany) equilibrated with purification buffer of pH 7.5 composed of 16.4 mM K_2HPO_4 , 3.6 mM KH_2PO_4 and 0.5 M NaCl containing 10 mM imidazole. Unbound and weakly bound fractions were eluted with purification buffer with 50 mM imidazole. Histidine-tagged protein was eluted with purification buffer with 300 mM imidazole. The eluted protein was dialysed against 50 mM phosphate buffer composed of 41 mM K_2HPO_4 , 9 mM KH_2PO_4 (pH 7.5). Protein concentrations were determined by the method of Bradford (Sigma-Aldrich, St. Louis, USA).

SDS-acrylamide electroforesis

SDS gel electrophoresis was run in 15 % acrylamide gels. The gels were stained by Coomassie brilliant blue R-250 stain (Fluka, Buchs, Switzerland) and molecular mass of proteins was determined based on Prestained SDS-Page Standards, Low Range (BioRad, Hercules, USA).

Activity assay

Hydrolytic dehalogenase activity of haloalkane dehalogenase DhIA and mutant protein DhIA01 was tested by spectrophotometric assay using the Iwasaki reagents (3). These solutions enable quantification of the concentration of halide ions released during the reaction. The 10 ml of 10 mM glycine buffer (pH 8.5) was pipetted to Erlenmeyer flasks. The buffer was incubated at 37 °C with halogenated substrate: 234 mM DCM, 13.19 mM DBM, 12.63 mM 1,2-dichloroethane (DCE) or 10.8 mM 1,2-dibromoethane (DBE). The reaction was stopped by adding of 1.0 ml of the reaction mixture to 100 µl of 35% HNO₃ in the time intervals 5, 10, 20 and 40 min, 2 hrs and 9 hrs after addition of enzyme. The Iwasaki reagents (100 µl and 200 µl) were added and absorbance of the mixture was measured by spectrophotometer at 460 nm.

Results:

Mutagenesis

The mutagenesis of *dhlA* gene was successful. It was confirmed that sequence contains only required substitution by sequencing on both strands (Fig. 1). Then the recombinant sequence was cloned into the pAQN expression vector.

Expression and purification

E. coli BL21 (DE3) cells containing plasmid carrying *dhlA* gene and mutant gene *dhlA01* were cultivated and recombinant proteins were purified (Fig.2). Expression of recombinant proteins was good, but proteins were not purified to homogeneity. The yield of both proteins was approximately 2 mg/l although the purity of proteins was not high. Purity and size (36.1 kDa) of both proteins were checked by SDS-PAGE (Fig. 3a, 3b).

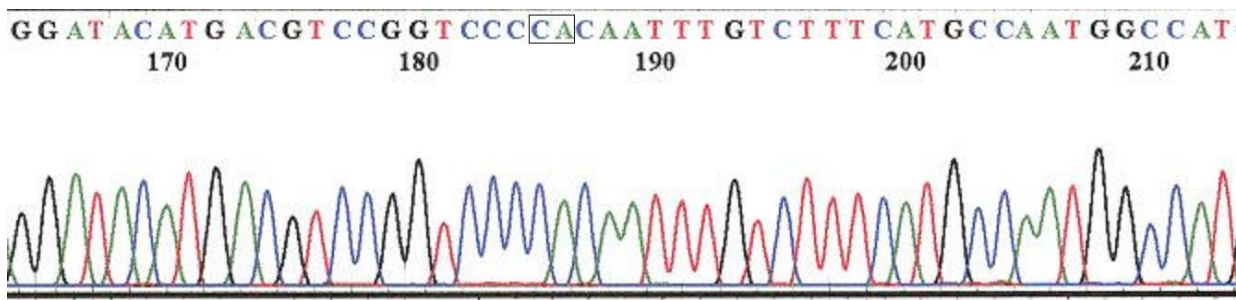


Fig. 1: Sequence analysis of mutant recombinant gene *dhlA01*. The substitution is in black box.

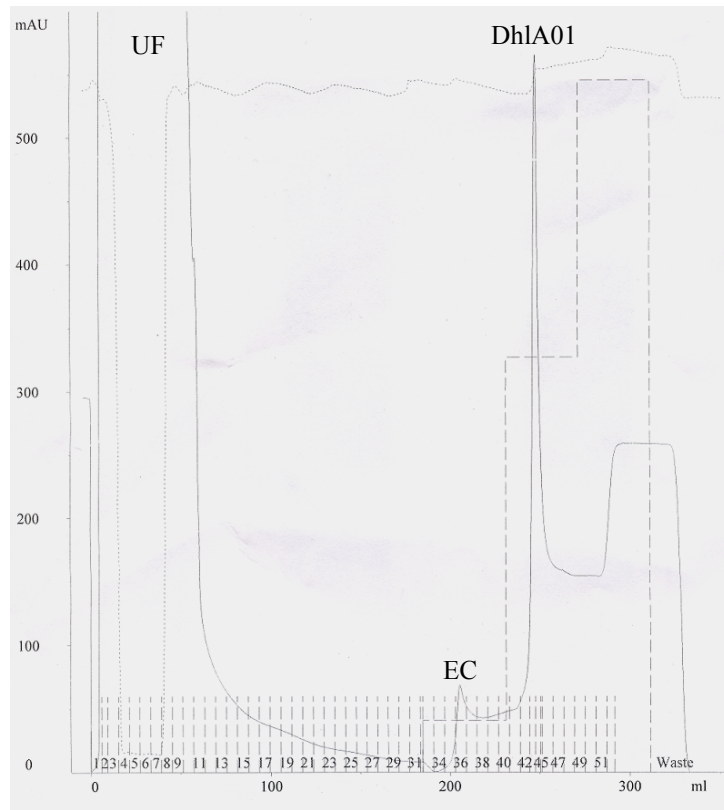


Fig. 2: Chromatogram from DhIA01 purification: UF - unbound fractions, EC - *E. coli* peak, DhIA01 – target protein peak.

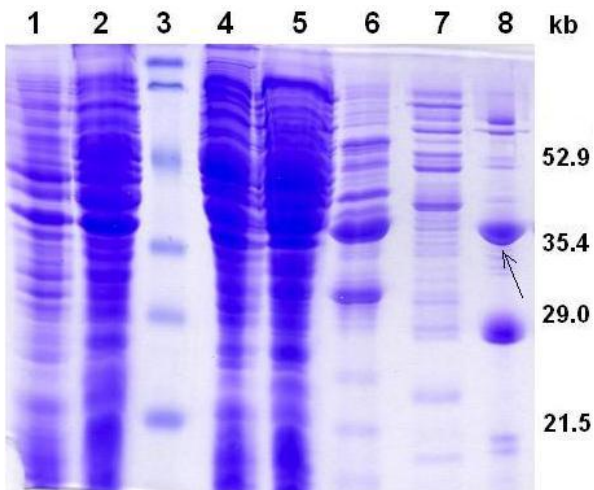


Fig. 3a: SDS acrylamide electroforesis of DhIA01. The DhIA01 band is marked by an arrow.

- 1 whole cells before induction
- 2 whole cells 4 hrs after induction
- 3 pre-stained SDS-Page Standard
- 4 crude extract
- 5 unbound fractions I
- 6 unbound fractions II
- 7 *E. coli* protein
- 8 DhIA01 protein

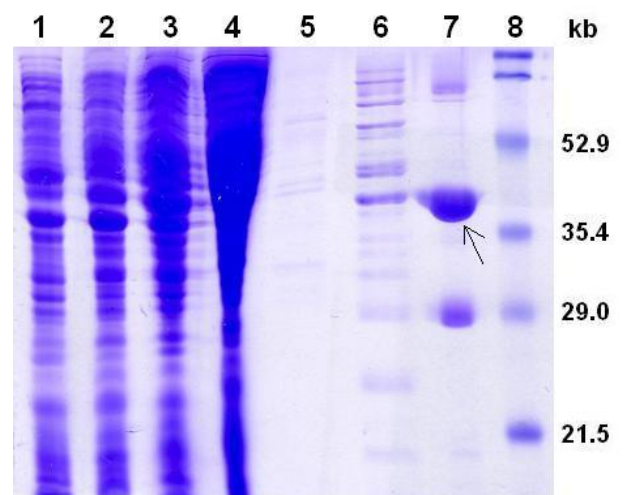


Fig. 3b: SDS acrylamide electroforesis of DhIA. The DhIA band is marked by an arrow.

- 1 whole cells before induction
- 2 whole cells 4 hrs after induction
- 3 crude extract
- 4 unbound fractions I
- 5 unbound fractions II
- 6 *E. coli* protein
- 7 DhIA protein
- 8 pre-stained SDS-Page Standard

Activity measurement

Kinetic parameters of wild type DhIA reported by Schanstra *et al.* (4) are listed in **Table 1**.

Tab. 1: Kinetic parameters of DhIA enzyme towards DCM, DBM, DCE and DBE reported by (4).

	chlorinated			brominated		
	K_m (mM)	k_{cat} (s^{-1})	k_{cat}/K_m ($M^{-1}s^{-1}$)	K_m (mM)	k_{cat} (s^{-1})	k_{cat}/K_m ($M^{-1}s^{-1}$)
CH ₂ X-CH ₂ X	0.53	3.3	6.2×10^3	0.01	3.0	3.0×10^5
CH ₂ X ₂	>100	-	0.70	2.4	3.9	1.6×10^3

Activity of purified proteins was tested by Iwasaki method on microtiter plates towards DCM, DBM, DCE and DBE (**Table 2, Figs. 4 and 5**).

Tab. 2: Comparison of specific activity values of wild type (DhIA) and mutant (DhIA01) determined by Iwasaki colorimetric assay.

Enzyme	Substrate	Slope	Specific activity ($\mu\text{mol}\cdot\text{s}^{-1}\cdot\text{mg}^{-1}$)
DhIA	DCM	0.0007	n.d.
	DBM	0.0135	0.046
	DCE	0.0178	0.053
	DBE	0.0199	0.069
DhIA01	DCM	0.0002	n.d.
	DBM	0.0007	n.d.
	DCE	0.0003	n.d.
	DBE	0.0242	0.005

DCM – 1,2-dichloromethane, DBM – 1,2-dibromomethane, DCE – 1,2-dichloroethane, DBE – 1,2-dibromoethane, n.d. – activity not detected.

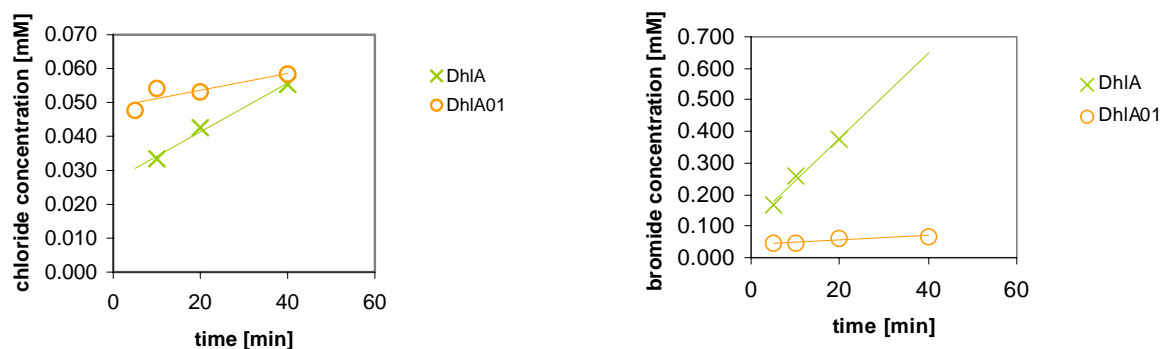


Fig. 4: Activity of DhIA and DhIA01 towards DCM (left) and DBM (right).

Both enzymes exhibited almost no activity towards DCM even after 9 hrs of catalysis. Visible activity was detected in case of its brominated derivate DBM and DCE with DhIA. Both DhIA and DhIA01 were active towards DBE. However, specific activity of DhIA01 was very low with this substrate. It is important to notice, that proteins were not purified into homogeneity so specific activities summarised in **Table 2** are underestimated. Moreover, it seemed that both enzymes were losing their activity over time. It might be necessary to use stabilizing reagents in DhIA samples for storage.

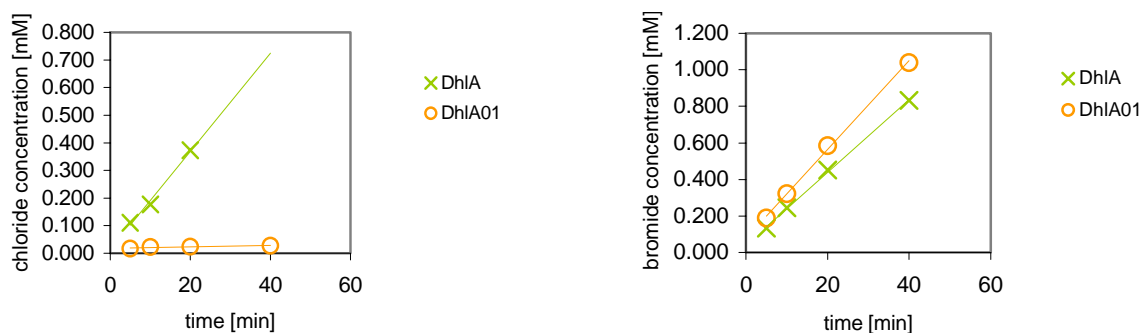


Fig. 5: Activity of DhIA and DhIA01 towards DCE (left) and DBE (right).

Conclusions:

Mutation L263W did not improve catalytic properties of DhIA towards DCM. Moreover, mutant protein DhIA01 lost its activity towards DBM and DCE, while its activity towards DBE was much lower compared to the wild type enzyme DhIA.

Acknowledgements:

I would like to thank Marta Monincová for valuable advices related to activity measurements and Andrea Jesenská for supervision and assistance.

References:

1. Klvaňa, M. (2005) Prediction of K_m of 1,1-dichloromethane (DCM) and 1,1-dibromomethane (DBM) for DhIA mutant L263W by using COMBINE model (progress report).
2. Nagata, Y., *et al.* (1999) *Prot Express Purif* 17, 229-304.
3. Iwasaki, I., *et al.* (1952) *Bull Chem Soc Jap* 25, 226.
4. Schanstra, J.P., *et al.* (1996) *J Biol Chem* 271, 14747-14753.

Equilibration Molecular Dynamics on DhaA with Products of 1,2,3-Trichloropropane Dehalogenation

Motivation:

Preparation of DhaA in a complex with products (chloride, Cl⁻, and (R/S)-2,3-dichloro-1-propanol, R/S-DCL) of dehalogenation of 1,2,3-trichloropropane (TCP) for study of product export routes.

Methods:

Preparation of Structures. Structures of DhaA.(Cl⁻).R/S-DCL were prepared previously by molecular docking using AUTODOCK 3.05 programme: R-DCL and S-DCL were docked into the active site cavity of free DhaA wild type (wt) structure and DhaA.Cl⁻ complex (Table 1). The chloride was bound between two halide-stabilising residues W107 and N41. Coordinates for the chloride were taken from 1CQW X-ray structure of DhaA with two iodide anions (one of them located between the two halide-stabilising residues, another one close to C176). The former iodide was replaced by single water molecule in DhaA.R/S-DCL. The latter iodide was replaced by single water molecule in DhaA.(Cl⁻).R-DCL and DhaA.Cl⁻.S-DCL; or was removed in DhaA.S-DCL. Crystallographic water molecules were added to the structures. Water molecules making steric clashes with the ligands were removed. Sodium counterions (17 Na⁺ for the systems without and 18 Na⁺ with Cl⁻) and rectangular parallelepiped box of TIP3P water molecules with closeness of 10 Å were added to the solutes using LEAP programme of AMBER 8.0 package (1).

Table 1. DhaA with products of dehalogenation of TCP.

Complex	Protein	Products
DhaA.R-DCL	DhaAwt	R-DCL
DhaA.S-DCL	DhaAwt	S-DCL
DhaA.Cl ⁻ .R-DCL	DhaAwt	Cl ⁻ and R-DCL
DhaA.Cl ⁻ .S-DCL	DhaAwt	Cl ⁻ and S-DCL

Equilibration Molecular Dynamics (MD). First, 300 steps of steepest descent method of energy minimisation was applied on hydrogen atoms of protein, ligands, counterions and all water molecules with the rest of the system restrained. The energy minimisation was followed by 20 ps molecular dynamics on counterions and all water molecules. Next, whole system was minimised in 4x300 steps of steepest descent with decreasing restraint on protein backbone (500, 125, 25 and 0). Finally, molecular dynamics was applied to the whole system with slow heating from 0 to 300 K during initial 200 ps using 2 fs time step. The SANDER module of AMBER 8.0 with the Cornell *et al.* force field (2) was used for all simulations. The particle-mesh Ewald method was employed for treatment of electrostatic interactions. The simulations were run under periodic boundary condition. The SHAKE algorithm was applied to fix all bonds containing hydrogen atoms. A 10.0 Å cutoff was applied for Lennard-Jones interactions. Coordinates were written into the trajectory files after each 0.5 ps. Stability of the systems were monitored by root-mean-square-deviation (RMSD) from X-ray structure and radius of gyration (GR). Systems were considered in equilibrium when both RMSD and GR curves were flat for hundreds of picoseconds. Three starting structures were selected for the

study of export routes for each complex. The starting structures were taken from last 300 ps of the MD, one starting structure per 100 ps. Time interval for the selection was extended to 600 ps for DhaA.Cl⁻.S-DCL (see Results).

Results:

DhaA.R-DCL. Total length of MD was 2.8 ns. RMSD was stable for last 900 ps with average value 1.45 Å² (Figure 1) and GR with average value 17.80 Å (Figure 2). R-DCL was stably bound and its hydroxyl group was making a hydrogen bond to D106-O_{δ1} during the whole simulation. Orientation of the catalytic water molecules was stable during MD as well. Three water molecules entered the active site cavity at ~230 ps (4843), ~1140 ps (473) and ~2600 ps (6457), and three water molecules left from the active site cavity at ~275 ps (692), ~1545 ps (4843) and ~2755 ps (6457). Water 473 was initially located in the slot, 692 in the active site cavity nearby C176; 4843 and 6457 were entering/leaving the active site cavity from/to bulk solvent through the main tunnel (4843) and the slot (6457). Starting structures for the study of export routes are snapshots at 2597 ps (A), 2699 ps (B) and 2791 ps (C). Structure A has open the main tunnel but closed the slot with W141, V245 and L246. Structure B has open both the main tunnel and the slot; there is one water in the slot (6457). Structure C has only the main tunnel. There are two water molecules in the active site cavity (309 and 473) in A, B and C structure.

DhaA.S-DCL. Total length of MD was 2.8 ns. RMSD was stable for last 900 ps with average RMSD 1.38 Å² (Figure 1) and GR 17.74 Å (Figure 2). R-DCL was bound by hydrogen bond between its hydroxyl group and D106-O_{δ1} during the whole simulation but it was less stable compared to R-DCL. Orientation of the catalytic water molecules was stable during MD. One water molecule entered the active site cavity through the slot at ~2202 ps (10202) and two water molecules escaped from the active site cavity through the slot at ~2030 ps (475) and ~2600 ps (10202). Water 475 was initially located in the slot. Starting structures for the study of export routes are snapshots at 2589 ps (A), 2700 ps (B) and 2800 ps (C). Structure A has open main tunnel but the slot is closed. Structure B has closed the main tunnel with T148 and K175 as well as the slot (there is only vesicule with water 474). Similarly, structure C has closed the main tunnel with A145 and C176 as well as the slot; there is just vesicule with water 474. There are two water molecules in the active site cavity (309 and 473) in A, B and C structure like in DhaA.R-DCL.

DhaA.Cl⁻.R-DCL. Total length of MD was 2.8 ns. RMSD was stable for last 800 ps with average RMSD 1.56 Å² (Figure 1) and GR 17.80 Å (Figure 2). R-DCL was stably bound by its hydroxyl group to Cl⁻ which is bound between the two stabilising residues W107 and N41 during the whole simulation. Orientation of the catalytic water molecules was stable only first 600 ps. The catalytic water (473) moved from its functional site at ~870 ps but water 1986 immediately (~875 ps) took its place for next ~55 ps. At ~930 ps 1986 moved away from the catalytic site. After ~1830 ps the site for the catalytic water became definitely occupied by water 693; its stability is, however, lower in comparison to the systems without Cl⁻ in the active site. Total of eleven water molecules entered the active site cavity and eight water molecules left the active site cavity throughout the simulation. Six out of 11 waters entered the active site cavity through the slot at ~240 ps (476), ~500 ps (475), ~725 ps (1986), ~425 ps (4455), ~710 ps (4348) and ~1425 ps (1997). Four out of 11 waters entered the active site cavity via main tunnel at ~220 ps (5496), ~595 ps (2412), ~1400 ps (5406) and ~2210 ps (3907). One water molecule (473) entered the active site cavity from the cavity for catalytic

water molecules at ~870 ps. Six out of eight water molecules escaped from the active site cavity via main tunnel at ~860 ps (2412), ~1260 ps (1986), ~1175 ps (4348), ~1255 ps (476), ~1425 ps (5406) and ~2325 ps (1997). Two water molecules left the active site cavity through the slot at ~1970 ps (473) and ~2605 ps (475). Starting structures for the study of export routes are snapshots at 2600 ps (A), 2700 ps (B) and 2800 ps (C). Structure A has open the main tunnel and the slot is missing. Structure B has open the main tunnel partially closed and the slot is missing. Structure C has open the main tunnel and closed slot by I135 and P210. Beside Cl⁻ and R-DCL, active site cavity of the structure A, B and C is occupied by four water molecules (693, 4455, 5496 and 3907).

DhaA.Cl⁻.S-DCL. Total length of MD was 2.2 ns. RMSD was stable for last 800 ps with average RMSD 1.39 Å² (Figure 1) and GR 17.85 Å (Figure 2). R-DCL formed temporary hydrogen bonds either with D106-O_{δ1} or Cl⁻ during the first 250 ps only. Afterwards, S-DCL was free to move in the active site cavity till the end of MD. S-DCL was mostly located either between F149 and C176 or close to H272 imidazole ring. Position of Cl⁻ between the halide-stabilising residues W107 and N41 was retained first ~1735 ps. Afterwards, interestingly, Cl⁻ left its binding site and the active site cavity through the main tunnel while S-DCL remained there. The process of Cl⁻ export took ~185 ps from ~1735 to ~1920 ps. After ~335 ps the catalytic water (473) moved from its functional cavity to Cl⁻ bound in the active site. Free space became occupied by another water (475; originally in the slot) at ~635 ps and kept its position till the end of the simulation. Total of nine water molecules entered the active site cavity and five water molecules left the active site cavity throughout the simulation. Three out of eight waters entered the active site cavity through the slot at the very beginning of MD: ~255 ps (474), ~275 ps (475) and ~280 ps (476). Five water molecules entered the active site cavity via the main tunnel at ~250 ps (3078), ~640 ps (5518), ~900 ps (7412), ~1405 ps (2795). One water molecule (694) escaped from the active site cavity before MD. Two water molecules did so via main tunnel at ~1750 ps (2795) and ~1925 ps (474). One water molecule left the active site cavity through the slot at ~1860 ps (5518). Starting structures for the study of export routes are snapshots at 1601 ps (A), 2125 ps (B) and 2200 ps (C). Structure A has main tunnel open and closed slot. The water 5518 is located in the bulge made of closed slot. Structure B has open the main tunnel and the slot is missing. Structure C has open the main tunnel and closed slot by I135, W141 and L246. Structure A contains both Cl⁻ and S-DCL in the active site cavity, and six water molecules (473, 474, 476, 2795, 3078 and 7412) plus one water in the bulge (5518). Structures B and C do not contain Cl⁻; active site cavity of B and C is occupied by S-DCL and four water molecules (473, 476, 3078 and 7412).

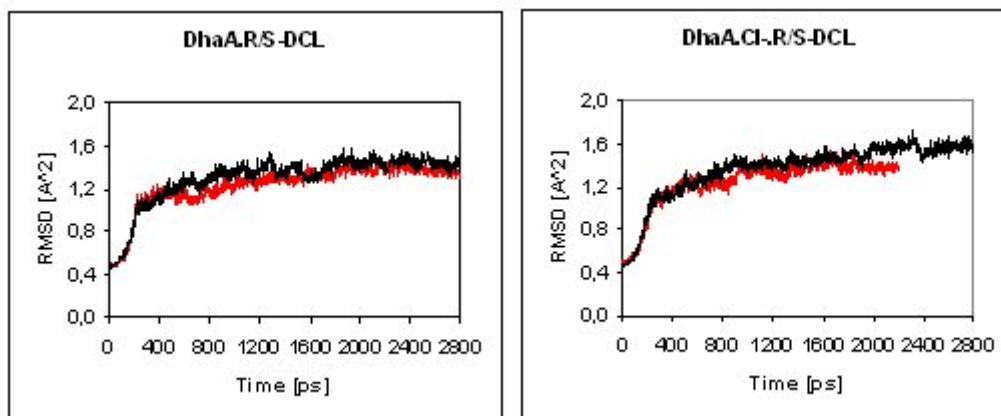


Figure 1. RMSD plots for MD. DhaA PDB-ID 1CQW with V172A+I209L+G292A was used as a reference structure. RMSD curves are coloured in black (R-DCL) and red (S-DCL).

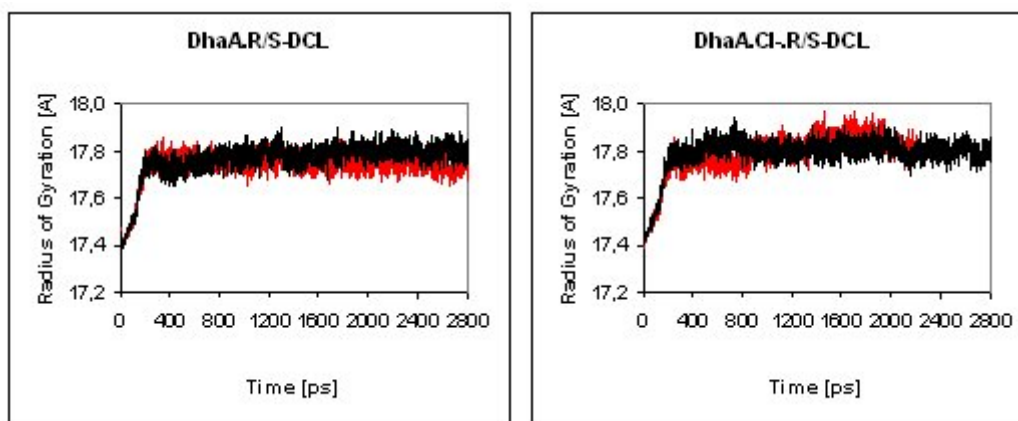


Figure 2. GR plots for MD. GR curves are coloured in black (R-DCL) and red (S-DCL).

Discussion:

Equilibrated complexes without Cl^- contain two water molecules in the active site cavity whereas systems with Cl^- have four water molecules in the active site. Cl^- bound in the active site strongly attracts water molecules first from slot then from main tunnel. DhaA.Cl $^-$.S-DCL simulation provided supportive evidence for an assumption that Cl^- leaves the active site before alcohol. This observation is in agreement with kinetic data determined with 1,3-dichloropropane) that export of an alcohol, but not Cl^- , is the rate limiting step of the overall reaction (3). Export of Cl^- from the active site is facilitated by several water molecules interacting with Cl^- via hydrogen bonds. Relevance of this observation is supported by flat RMSD curve indicating stable system. Average RMSD of the equilibrated DhaA.Cl $^-$.S-DCL was 1.39 Å compared to 1.56 Å for analogous system with R-DCL and the RMSD is almost the same as for DhaA.S-DCL (1.38 Å). In distinction to Cl^- , S-DCL stucked in the active site cavity probably because of favourable interactions with H272 imidazole ring and too narrow mouth of the main tunnel formed predominantly by C176 and F149.

In case of DhaA.Cl $^-$.R-DCL such a striking escape of Cl^- was not observed most probably due to different orientation of R-DCL from molecular docking: R-DCL is oriented towards the slot reducing conformational freedom of the molecule. Unlike R-DCL, S-DCL is

oriented towards the main tunnel thus it is much more free to move in the active site cavity. Indeed, S-DCL interacts with D106-O_{δ1} and Cl⁻, respectively, only during first 250 ps enabling access of waters to Cl⁻ and destabilisation its position between the halide stabilising residues. A question arises whether the difference between R-DCL and S-DCL is just an artefact of the docking procedure or whether it has a natural foundation.

The most attractive complex for study of export routes is DhaA.Cl⁻.S-DCL system without Cl⁻, i.e. only with S-DCL located freely in the active site cavity enabling use of much smaller acceleration constant compared to other complexes containing R/S-DCL bound via hydrogen bond to either Cl⁻ or D106-O_{δ1}. Furthermore, the product of TCP dehalogenation is expected to stack on H272 ring as observed for S-DCL from DhaA.Cl⁻.S-DCL system. The expectation has a substantiation in experimentally solved X-ray structure of LinB with R-DCL (4) in which the most striking interactions of R-DCL with the active site residues are the contacts with the catalytic histidine that must provide strong van der Waals interaction between the ligand molecule and H272 ring. The same interaction will be present also in DhaA based on identical position and orientation of catalytic histidine within the tunnel opening.

Conclusions:

- DhaA in complex with products (Cl⁻ and (R/S)-2,3-dichloro-1-propanol) of dehalogenation of 1,2,3-trichloropropane (TCP) was prepared for study of product export routes using several steps of energy minimisations and MD simulations.
- All four prepared complexes are suitable for study of export routes. However, the most relevant complex seems to be DhaA.Cl⁻.S-DCL after release of Cl⁻.
- R/S-DCL from DhaA.R/S-DCL complexes established a hydrogen bond with D106-O_{δ1} the active site cavity, while R-DCL from DhaA.Cl⁻.R-DCL complex formed stable hydrogen bond with Cl⁻. S-DCL from DhaA.Cl⁻.S-DCL complex moved from the hydrogen bonding interactions with D106-O_{δ1} and Cl⁻ about 50 ps after heating phase of the equilibration MD. Then it stacked on H272 ring for the rest of the MD simulation.
- Cl⁻ in DhaA.Cl⁻.S-DCL complex (but not in DhaA.Cl⁻.R-DCL) left its binding site and the active site cavity through the main tunnel.
- Proper position and orientation of catalytic water molecule is retained in DhaA.R/S-DCL complexes while in DhaA.Cl⁻.R/S-DCL systems the catalytic water molecule moved towards Cl⁻. Its place became immediately occupied by another water molecule. Such exchange occurred once in DhaA.Cl⁻.S-DCL and twice in DhaA.Cl⁻.R-DCL.
- The active site cavity is connected to the surface via the main tunnel and the slot. Both of them could adopt open and closed state during various simulations. Residues involved in closure of the main tunnel are F144, A145, F149, A172 and C176. The slot can be blocked by R133, I135, W141, P210, V245 and L246.

References:

1. Case, D.A., *et al.* (2004) AMBER 8, University of California, San Francisco.
2. Cornell, W.D., Cieplak, P., Bayly, C.I., Gould, I.R., Merz, K.M., Ferguson, D.M., Spellmeyer, D.C., Fox, T., Caldwell, J.W., and Kollman, P.A. (1995) *JACS* 117, 5179-5197.
3. Bosma, T., Pikkemaat, M. G., Kingma, J., Dijk, J., and Janssen, D.B. (2003) *Biochemistry* 42, 8047–8053.
4. Banáš, P., Otyepka, M., Vévodová, J., Jeřábek, P., Boháč, M., Petřek, M., and Damborský, J. (2005) submitted.

Development of Measurement Cell for Biosensors

Motivation:

The need of measurement cell development emerged during the first experiments using pH optode for enzymatic activity monitoring when the instability of pH optode signal and the insufficient reproducibility of kinetic data were observed.

Requirements:

temperature control: speed of enzymatic reaction is strongly dependent on temperature

1. closed system: majority of target halogenated compounds are volatile
2. stirring: fast mixing of enzyme with substrate and keeping homogenous conditions
3. fixed access tube and titrant delivery needle: avoid the disturbance of pH optode signal observed during titration of enzyme in and/or withdrawing a sample out of the measurement vial during first experiments; pH optode protection against mechanical damage

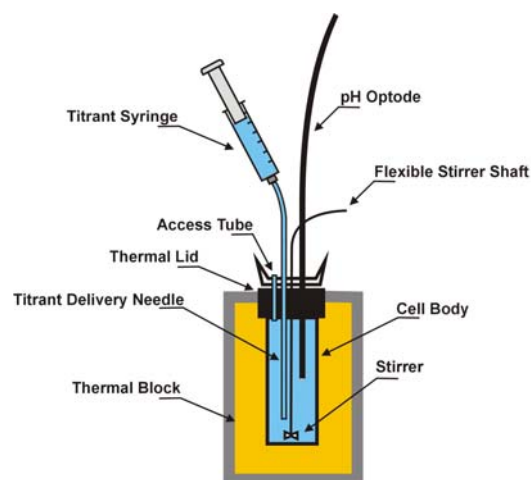
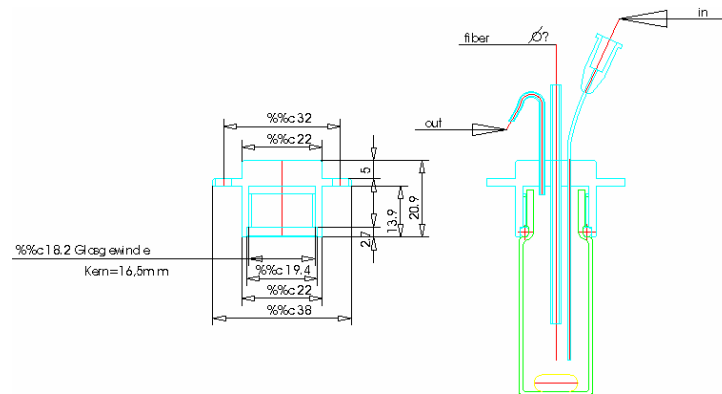


Figure: Thermostated cell for enzyme activity measurement using pH optode

